# Electron Tunneling Across Hexadecanethiolate Monolayers on Mercury Electrodes: Reorganization Energy, Structure, and Permeability of the Alkane/Water Interface

**Krzysztof Slowinski, Katarzyna U. Slowinska, and Marcin Majda***

*Department of Chemistry, University of California at Berkeley, Berkeley, California 94720-1460*

*Received: May 5, 1999; In Final Form: August 4, 1999*

Measurements of the reorganization energies ($\lambda$) and the maximum values of the electron transfer rate constants ($k_{app}^{max}$, obtained for $-\eta \geq 2\lambda$) of two redox probes at monolayer-coated electrodes are used as diagnostic parameters of the location of a probe at the monolayer/solution interface. Kinetics of the electroreduction of $IrCl_6^{2-}$ and $FcCH_2N(CH_3)_3^{2+}$ at hexadecanethiolate-coated Hg drop electrodes were investigated in a broad range of overpotentials extending to values in excess of the reorganization energies of the two redox probes. Rate vs overpotential data were analyzed in terms of the Marcus−Gerischer formalism to yield the reorganization energies and $k_{app}^{max}$ values. The former show that both probes reside initially in an aqueous environment at the alkane/solution interface. A larger value of $k_{app}^{max}$ for the ferrocene probe was interpreted to indicate its closer approach to the interface. Access of the more strongly hydrated $IrCl_6^{2-}$ to the interface is more restricted by an interfacial water layer. Gradual expansion of the Hg drop, up to 20% of its initial surface area, has no effect on the magnitude of the reorganization energy obtained for $IrCl_6^{2-}$, proving that the iridium probe is located in the aqueous environment outside the alkane monolayer film. In contrast, a more hydrophobic ferrocene probe permeates the alkanethiolate monolayer immediately when even a small expansion of the Hg drop of ca. 2% is attempted.

## Introduction

Dependence of the kinetics of long-range electron transfer on the structure of a molecular fragment bridging electron donor and acceptor is not well understood.[1−3] Yet, efficient, bridge-mediated, electron tunneling is ubiquitous in biological processes[2−9] and is of crucial importance in the rapidly growing area of molecular electronics.[10−12] In the nonadiabatic limit of the Fermi's golden rule, the rate of electron transfer depends on the bridge-mediated electronic coupling between donor and acceptor ($H_{DA}^2$) and the Franck−Condon density of states (FC):[13]

$$k_{et} = (2\pi/\hbar)H_{DA}^2(\mathrm{FC}) = (2\pi/\hbar)H_{DA}^2(4\pi\lambda k_B T)^{-1/2} \exp[(-(\Delta G^\circ + \lambda)^2/(4\lambda k_B T)] \quad (1)$$

The Franck−Condon factor features the values of a reaction free energy and the reorganization energy ($\lambda$). The electronic coupling matrix element depends on the length and the molecular structure of the bridge. The mediating efficiency of the bridge is expressed by the magnitude of the decay constant $\beta$ in a well accepted equation expressing an exponential decrease of $H_{DA}^2$ with the donor−acceptor distance,

$$H_{DA}^2(d) = H_{DA}^2(d{=}0)\exp(-\beta d) \quad (2)$$

It is noteworthy that an increasing volume of experimental data suggests, contrary to earlier postulates,[14] that in biological as well as synthetic systems, $H_{DA}^2$ reflects the length and structure of a specific *tunneling pathway* rather than a simple geometric D−A spacing.[9,15−24]

Recent electrochemical measurements of electron tunneling kinetics have provided detailed information concerning intervening medium effects for several simple systems.[22,24−30] In these types of experiments, approach of a redox probe to the electrode surface is restricted to a specific distance by an impermeable monolayer film at the electrode/solution interface. Self-assembled alkanethiol type monolayers on gold are the best examples of a tunneling barrier film. Variation of the alkane chain length allows one to examine the distance dependence of the electron-transfer rate constant. Interpretation of such measurements in terms of $\beta$ required identification of a specific tunneling pathway. Since in these monolayers, the alkane chains are known to be tilted by ca. 30°,[31] the geometric film thicknesses are substantially smaller than the length of the alkane chains. Assuming, nevertheless, that the major pathway across these films involves tunneling through $\sigma$-bonds, decay constants in the range 0.78−0.97 Å$^{-1}$ were reported.[27−30] The influence of atomic level modifications in the structure of the alkane chains was also investigated.[22] Specifically, replacement of one methylene unit by ether, olefine, or alkyn fragments decreased the electronic coupling across the monolayer.[22] More recently, electrochemical tunneling experiments involving other $\sigma$- and $\pi$-bonded bridges such as those composed of a string of phenylethynyl units have also been probed.[32,33] Due to the extended nature of the electronic orbitals in these conjugated molecular fragments, substantially smaller $\beta$ values (0.36−0.57 Å$^{-1}$) were obtained.[32,33]

Recent use of mercury as the electrode material in electron tunneling experiments has brought about several advantages.[23,34−36] Mercury offers an atomically smooth, defect free, and highly reproducible surface for alkanethiol self-assembly. More importantly, we have demonstrated recently that gradual expansion of a suspended Hg drop[37] coated with an alkanethio-

* Corresponding author. E-mail: majda@socrates.berkeley.edu.

10.1021/jp991466a CCC: $18.00 
Published on Web 09/15/1999

late monolayer (in the range of $C_{10}SH$ to $C_{16}SH$) results in a decrease of the monolayer thickness without generating pinhole defects.[24] The decrease of the film thickness was inversely proportional to the increase of the drop surface area. This liquidlike character of these monolayers was accounted for by postulating that all alkanethiolate molecules adopt a gradually increasing average tilt as the film is expanded. In the course of electrochemical measurements, we have discovered that a large (ca 25%) decrease of the geometric film thickness resulted only in a small increase (an order of magnitude smaller than expected) of the tunneling rate.[24] Clearly, alkanethiol monolayers cannot be treated as isotropic tunneling barriers. These experiments proved that the predominant pathway of electron tunnelling involves $\sigma$-bonded alkyl chains, a pathway invariant in length regardless of the tilt angle of the alkyl chains. We have shown further that the small increase of the tunneling current observed in the course of a Hg drop expansion can be accounted for by postulating the existence of an additional tunneling pathway involving chain-to-chain coupling. Quantitative analysis of our data yielded a "through-space" decay constant characterizing that coupling, $\beta_{ts} = 1.3$ Å$^{-1}$. The higher value of this decay parameter reflects substantially smaller coupling strength between two adjacent alkyl chains. It is equivalent to the coupling along 5.5 $\sigma$-bonded methylene units of an alkyl chain.

While the experiments summarized above yielded the first direct measurements of the coupling strength across a nonbonded, van der Waals bridge, the data analysis that was used to interpret the measurements involved an assumption that the redox probe ($Ru(NH_3)_6^{3+}$) remained outside the monolayer/solution interface. In other words, it was assumed that that the probe did not penetrate the alkane medium of the monolayer film to any extent. The latter event, if it had taken place, would result in a shorter tunneling distance. This could account for the small increase of the tunneling current. In this report, we outline an experimental approach designed to address this crucial question.

Knowledge of the precise location of a redox probe at a monolayer/solution interface and consequently the exact length of a tunneling pathway across a barrier film at the electrode surface are naturally of crucial importance in the interpretation of electron tunneling data. In monolayer systems in which a redox probe is covalently tethered to the bridging group itself, the tunneling distance is usually sharply defined if the all-trans conformation of the bridging alkane chains can be assured.[26,29,30] However, in cases where redox probe species are free to diffuse in the contacting solution, an experimental strategy that is synthetically easier to implement and one that offers substantial flexibility in selecting redox probes, their location at the monolayer/solution interface is a priori less well-known.[22,24,28,38−41] As mentioned above, this is of particular importance in our Hg drop expansion experiments in which a large surface area increase and the concurrent monolayer expansion could easily generate pinhole defects that would allow a redox probe to move closer to the electrode surface than the average film thickness. In Figure 1, we show two opposite scenarios that may be envisioned upon monolayer expansion. Case A depicts a situation postulated in our previous report,[24] namely, that an expansion of an alkanethiolate monolayer coated Hg drop results in a progressively large average tilt of the alkane chains without generating pinhole defects. In case B, pinhole defects allow closer access of a redox probe to the electrode surface. In the approach presented below, we record kinetically controlled current for the reduction of two redox probes over a large range of overpotentials. Using the Marcus−Gerischer formalism, we

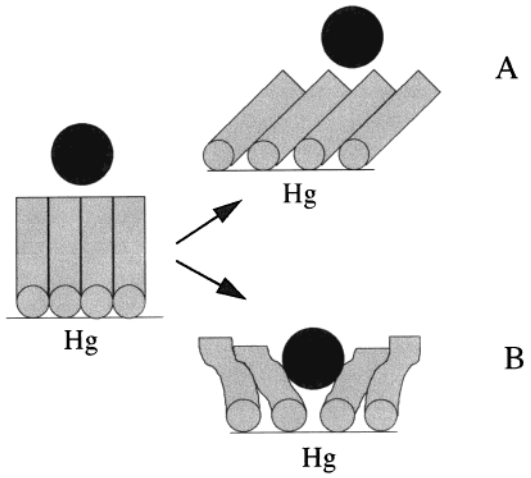


**Figure 1.** A schematic representation of two different structures of an alkanethiolate monolayer adopted upon expansion of a Hg drop electrode. (A) The monolayer is essentially pinhole free. A redox probe is located outside the monolayer/solution interface. The chains exhibit a tilt adopted in response to monolayer expansion. **(**B) Hg drop expansion results in formation of pinhole defects. A redox probe can partially permeate the alkane region of the monolayer.

carry out measurements of the reorganization energy, $\lambda$, of the redox probes.[26,40,42] These measurements allow us to determine their position at the monolayer/solution interface and thus to distinguish between the two scenarios shown in Figure 1. We demonstrate that whether the probe is hydrophilic or hydrophobic is a key factor in determining its behavior at the interface.

Two redox probes were selected to be used in these experiments, $IrCl_6^{2-/3-}$ and a ferrocene derivative, $FcCH_2N(CH_3)_3^{2+/+}$. Their reorganization energies are dominated by the outer-sphere terms and therefore depend strongly on the dielectric properties of the surrounding medium. For example, a probe remaining in the aqueous environment during a monolayer expansion, as shown in Figure 1, case A, will report the same $\lambda$ value throughout an expansion experiment. A substantial decrease of $\lambda$ is expected if a probe permeates even partially into the alkane medium of the monolayer, as in case B in Figure 1. In our selection of the redox probes we wanted to evaluate the effect of their hydrophobicity on the extent of permeation through the monolayer films. Clearly, $FcCH_2N(CH_3)_3^{2+}$ is a more hydrophobic ion than $IrCl_6^{2-}$. In addition to the reorganization energies, our measurements yield also the maximum values of the rate constants, $k_{app}^{max}$. Comparison of the $k_{app}^{max}$ values for the two probes with the literature $k_{app}^{max}$ values obtained in similar experiments for a number of other redox species[42] allows us to draw further conclusions regarding their relative location at the monolayer/solution interface.

## Experimental Section

Fresh samples of hexadecanethiol were purchased from Aldrich. They were used as received. Mercury (Quicksilver Products Inc., triply distilled) was used without further purification. The following reagents were also used as received: ethanol (Fisher, reagent grade), KCl (Fisher, ACS grade), $Na_2IrCl_6$ (Strem, 99%), $NaClO_4$ (Fisher, purified), $HClO_4$, (Seastar, double sub-boiling distilled in quartz). $FcCH_2N(CH_3)_3PF_6$ has been prepared by mixing saturated solutions of ammonium hexafluorophosphate (Strem) and ferrocenylmethyltrimethylammonium iodide (Strem). The precipitate, $FcCH_2N(CH_3)_3PF_6$, was subsequently recrystallized three times from water. The oxidized form of $FcCH_2N(CH_3)_3PF_6$ was generated electrochemically by preparatory electrolysis.

A Kemula−Kublik type hanging mercury drop electrode[43] was constructed using a design described by Guidelli and coworkers.[44] A more detailed description of the electrode and of its performance was presented previously.[24] Self-assembly of hexadecanethiolate monolayers on Hg was carried out from saturated ethanolic solutions. The incubation time was typically 2 min. Longer incubation times, up to 20 min, did not induce any changes in the properties of the resulting monolayer films. Following self-assembly, the electrode was carefully rinsed with ethanol for 10 s and with water for 5 s and then transferred into the electrochemical cell with an aqueous electrolyte. All electrochemical measurements were done with a BAS 100A electrochemical analyzer, using a two-compartment cell at room temperature of 20 °C. The voltammetric tunneling currents were corrected digitally by subtracting capacitive current. All potentials were measured and are reported vs saturated calomel reference electrode (SCE).

## Results and Discussion

**Electrochemistry in the Marcus Inverted Region**. Self-assembly of long alkyl chain thiols (with the chain length greater than $C_8$) on mercury leads to the formation of well behaved, impermeable alkanethiolate monolayer films.[24,34−36,45] Consistent with X-ray reflectivity data,[46] our coulometric measurements showed that the orientation of the alkyl chains is close to vertical, with densities approaching close packed structures (average area of ca. 20 Å$^2$/molecule were obtained).[24] Despite these rather high packing densities, monolayers with the number of carbon atoms in the range 9−16 appear to be liquid, and can be expanded by increasing the volume of a mercury drop electrode. Unlike octadecanethiolate monolayers, which tear upon even small expansion to generat defects, shorter chain monolayers maintain their impermeable characteristics even upon sizable (25−30%) expansion.[24] Their presence on the mercury surface inhibits Hg oxidation and therefore widens substantially the accessible range of positive potentials.[34] The negative limit of a potential range is set by the onset of reductive desorption of an alkanethiolate monolayer. Both the positive and negative limits of accessible potentials depend on the chain length of the alkanethiols used to form the monolayer film. With the hexadecanethiolate films investigated in this report, the accessible range of potentials extends approximately from 0.70 V (0.6 in 0.5 M KCl solutions) to −0.70 V. In this range, the interfacial capacitance of ca. 0.8 $\mu$F/cm$^2$ is essentially independent of the electrode potential, reflecting the invariance of the two monolayer properties of dielectric constant and film thickness.[24] These characteristics allow us to study electron transfer kinetics across these barrier films in a broad range of potentials. This is crucial to our goal as we set out to measure rates of electron transfer over a wide range of overpotentials.

We first deal with iridium hexachloride ($IrCl_6^{2-/3-}$). This hydrophilic, outer-sphere probe has a formal potential of +0.727 V and a large standard heterogeneous electron transfer rate constant of 0.5−2 cm/s.[47−49] Its reduction on a hexadecanethiolate coated Hg ($Hg/C_{16}$) drop electrode is shown in Figure 2. As expected for a thick barrier film, an overpotential ($E - E^{\circ\prime}$) in excess of −0.5 V is necessary to observe a measurable reduction current. As the magnitude of the driving force approaches and exceeds the reorganization energy (which typically is on the order of 1 eV for these types of redox probes), the current exhibits a Marcusian curvature as the rate of increase of the overlap between the density of electronic states in the metal and a population of $IrCl_6^{2-}$ at the $Hg/C_{16}$/solution interface decreases (see the discussion below).[13,42] Indeed, development

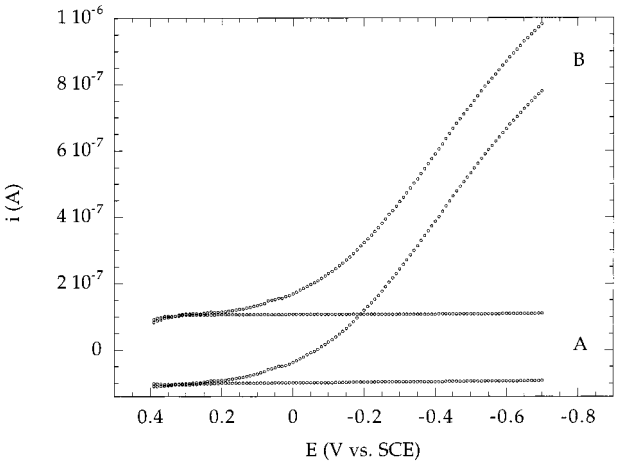


**Figure 2.** Current−voltage curves recorded with a hexadecanethiolate-coated Hg drop electrode in 0.5 M KCl solution in the absence (A) and in the presence (B) of 1.0 mM $IrCl_6^{2-}$; $v = 5.12$ V/s. Electrode surface area, $A = 0.0246$ cm$^2$.

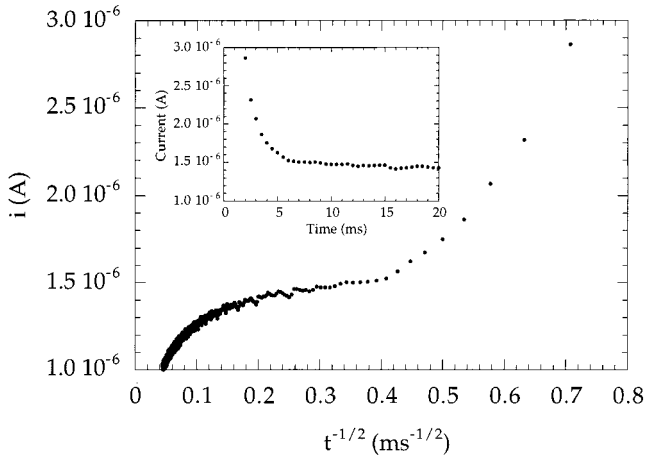


**Figure 3.** Plot of $i$ vs $t^{-1/2}$ for a chronoamperometric transient recorded in a 0.5 M KCl solution containing 1.0 mM $IrCl_6^{2-}$ with a hexadecanethiolate-coated Hg drop electrode. The potential (a 500 ms pulse) was stepped from +0.4 to −0.7 V vs SCE. The inset shows the $i-t$ data recorded during the first 20 ms of the experiment.

of a plateau in these electrochemical experiments corresponds to Marcus' inverted region for homogeneous electron transfer reactions. Since, in our experiment, the electrode with a continuum of electronic states at and below the Fermi level plays the role of the electron donor, decrease of the rate of electron transfer is not observed, simply because tunneling from the states below the Fermi level is possible at overpotentials in excess of $\lambda$.[13,42]

Naturally, these statements hold only in cases where the observed current is limited by the electron transfer kinetics and not by mass transport. We have two pieces of evidence to prove this is indeed the case. First, the reduction current in Figure 2 was recorded at a sufficiently high scan rate (>5 V/s) to make it scan rate independent. In other words, under the conditions of Figure 2, the rate of diffusive mass transport of $IrCl_6^{2-}$ to the monolayer/solution interface is at least 20 times faster than the rate of electron transfer.[50] To further probe this relationship, we carried out chronoamperometric measurements in which a large potential pulse (from 0.40 V, where no current flows, to −0.70 V) is applied to the $Hg/C_{16}$ electrode immersed in a $IrCl_6^{2-}$ solution. A typical current−time response is shown in Figure 3. Three regions can be identified: for $t < 5$ ms, a decreasing current is due to the charging of the $Hg/C_{16}$/solution

interface. The same current was also obtained in this time interval in the absence of the $IrCl_6^{2-}$. Second, the current becomes essentially independent of time for a short interval between ca. 7 and 15 ms (see the inset in Figure 3). In this region, the current is controlled by the constant rate of electron tunneling across the hexadecane monolayer. At longer times ($t$ > 15 ms), the rate of diffusion of $IrCl_6^{2-}$ to the $Hg/C_{16}$/solution interface progressively decreases and ultimately becomes the rate-limiting process. In view of the Cottrell equation describing diffusion controlled electrode reactions, in that range the current should decrease as $1/\sqrt{t}$.[51] This is indeed observed in Figure 3 at times greater than 0.1 s.

The significance of this experiment is two-fold. First, the time interval during which the current is independent of time $\tau$ (7−15 ms) allows us to identify the lowest scan rate in voltammetric experiments that would ensure that electron transfer is a rate-limiting step. In view of $\tau = RT/nF\upsilon$, the corresponding scan rate ($\upsilon$) must be $\upsilon$ > 3.9 V/s. The scan rate used in the experiment of Figure 2 is, indeed, of sufficiently high magnitude. More important is the analysis of the entire temporal dependence of the Faradaic current (at $t$ > 7 ms in Figure 3). It is only fair to point out that time-independent current could also be observed in our chronoamperometric experiments if the hexadecane monolayer film were populated with a number of widely spaced pinhole defects. The electrode would function then as an array of independent microelectrodes that is known to exhibit steady-state currents. However, in such a case, a true steady-state would develop. A rapid onset of diffusion control and a decrease of current at $t$ > 15 ms clearly eliminates the possibility of pinhole diffusion. Thus, these chronoamperometric experiments ensure us that the voltammetric current in Figure 2 represents the rate of electron tunneling across the hexadecanethiolate monolayer. The rate constant of this process, $k_{app}$ is readily obtained from the measured current,

$$k_{app}(E) = i(E)/nFAC^*_{IrCl_6^{2-}} \qquad (3)$$

where $F$ is the Faraday constant and $C^*_{IrCl_6^{2-}}$ is the bulk concentration of $IrCl_6^{2-}$.

**Analysis of the Experimental Data and Determination of a Correlation between $k_{app}^{max}$ and $\lambda$.** Next, we interpret $k_{app}(E)$ data in terms of the reorganization energy and related parameters. Similarly to $k_{et}$ in eq 1, the electrochemical rate constant $k_{app}(E)$ may be expressed in terms of the electronic coupling ($H_d^2(E) = H_0^2(E)\exp(-\beta d)$) between the redox species and the electrode surface and the overlap of the density of electronic states on both sides of the interface, $\rho$(ox) and $\rho$(metal).[42] For a nonadiabatic process, the later involves the density of all filled states in the metal $\rho$(metal);

$$\rho(\text{metal}) = \frac{1}{\exp[(E - E_F)/kT] + 1} \qquad (4)$$

In view of the Marcus theory, the redox density of states distribution is a Gaussian,

$$\rho(\text{ox}) = (4\pi\lambda k_B T)^{-1/2} \exp[-(\lambda - e\eta)^2/4\lambda k_B T] \qquad (5)$$

Thus, overall

$$k_{app}(E) = (4\pi^2/h)(4\pi\lambda k_B T)^{-1/2} \int_{-\infty}^{+\infty} \{\rho(\text{metal}) H_0^{\,2}(E) \exp(-\beta d) \exp[-(\lambda - e\eta)^2/4\lambda k_B T]\}\, dE \qquad (6)$$

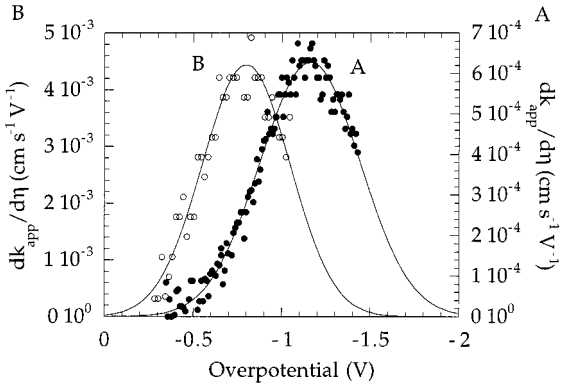


**Figure 4.** Plots of $dk_{app}/d\eta$ vs $\eta$ (overpotential) for the reduction of $IrCl_6^{2-}$ (A) and $FcCH_2N(CH_3)_3^{2+/+}$ (B). The $k_{app}$ vs $\eta$ data were obtained under the conditions of Figures 2 and 5. The lines correspond to the Gaussian fits through the data. The fitting parameters are listed in Table 1.

**TABLE 1: Kinetic Parameters of the Redox Probes Obtained with $Hg/C_{16}$ Electrodes**

| redox probe | $E^{\circ\prime}$ (V) vs SCE[a] | $\lambda_{Ox}$ (eV)[b] | $k_{app}^{max}$ (cm/s)[b] |
|---|---|---|---|
| $IrCl_6^{2-/3-}$ | +0.727 | 1.16 ± 0.01 | $(4.5 \pm 1.0)\cdot 10^{-4}$ |
| $FcCH_2N(CH_3)_3^{2+/+}$ | +0.380 | 0.80 ± 0.03 | $(2.7 \pm 1.5)\cdot 10^{-3}$ |

[a] Measured at a clean glassy carbon electrode in the electrolyte solutions of Figure 5. [b] The values of $\lambda$ and $k_{app}^{max}$ represent the averages and standard deviations of 10 independent measurements carried out with different $Hg/C_{16}$ electrodes.

Assuming that the Fermi distribution is a step function and that $H_0(E)$ and $\beta$ are independent of the electrode potential, it becomes possible to differentiate both sides of eq 6 with respect to $\eta$ to obtain

$$dk_{app}/d\eta = (4\pi^2/h)\,\rho H_d^{\,2}(4\pi\lambda kT)^{-1/2} \exp[-(\lambda - e\eta)^2/4\lambda kT] \qquad (7)$$

Thus, $dk_{app}/d\eta$ is also a Gaussian. A plot of $dk_{app}/d\eta$ vs $\eta$ for the reduction of $IrCl_6^{2-}$ is shown in Figure 4. The reorganization energy and the maximum value of the rate constant ($k_{app}^{max}$) are obtained as the fitting parameters. $k_{app}^{max}$ is a plateau value of the rate constant at the infinitely negative overpotentials (ca. $-\eta \geq 2\lambda$).[42] Thus, it is independent of the reorganization energy of a redox probe and represents only the strength of the electronic coupling across the tunneling barrier film (and $\rho$(metal), a constant term). The values of $\lambda$ and $k_{app}^{max}$ are listed in Table 1.

The same voltammetric experiments were also carried out for the reduction of the second, more hydrophobic redox probe selected for these investigations, $FcCH_2N(CH_3)_3^{2+/+}$ ($E^{\circ\prime}$ = 0.380 V).[52] The comparison of the $k_{app}$ vs overpotential data (obtained from the background corrected, kinetically controlled voltammetric reduction currents according to eq 3) for both probes is shown in Figure 5, while Figure 4 presents the two corresponding $dk_{app}/d\eta$ vs $\eta$ plots. The reorganization energies for both probes (Table 1) are in a good agreement with previous electrochemical measurements[26,53] and with the Marcus dielectric continuum model for an aqueous environment.[13] This model is appropriate for calculating $\lambda$'s for the outer-sphere redox probes. For ferrocene in an aqueous environment, it gives $\lambda$ = 0.95 eV using the accepted value of 3.8 Å for the radius of ferrocene. Earlier measurements obtained for ferrocene covalently attached to alkanethiol monolayers on gold yielded $\lambda$ of ca. 0.85 eV.[26,53] Those authors argued that their measurements were low, due to the fact that the ferrocene probe was attached

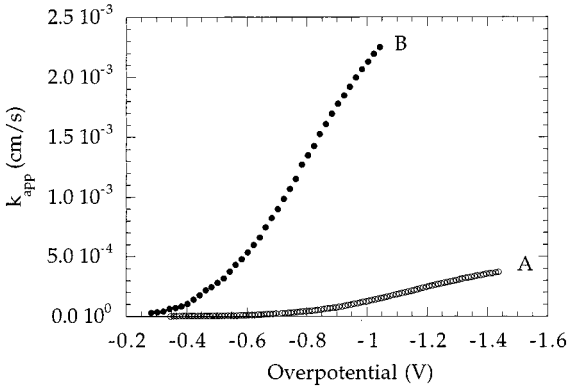


**Figure 5.** Plots of $k_{app}$ vs overpotential for the reduction of $IrCl_6^{2-}$ (A) and $FcCH_2N(CH_3)_3^{2+/+}$ (B). The data were obtained from the respective $i-V$ curves such as those in Figure 2. Voltammograms for the reduction of the ferrocene probe were recorded with a hexadecanethiolate-coated Hg drop electrode in a pH = 3.0, 0.2 M $NaClO_4$ solution containing 1.0 mM $FcCH_2N(CH_3)_3^{2+}$ at $\nu$ = 20.48 V/s.

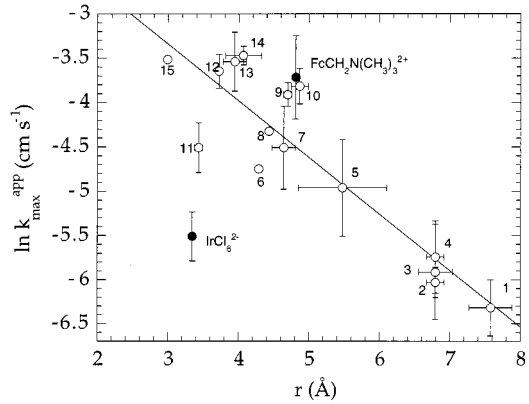


**Figure 6.** Correlation of $\ln(k_{app}^{max})$ vs $r_{app}$ data for a number of transition metal complexes (open circles) obtained by Miller et al. at the $\alpha,\omega$-hydroxytetradecanethiol-coated Au electrodes (see ref 40) and for $IrCl_6^{2-}$ and $FcCH_2N(CH_3)_3^{2+}$ (Fc). The latter two $k_{app}^{max}$ values were scaled to correct for the difference in the alkanethiolate chain lengths used in Miller's and our experiments (see text and ref 57). In all cases, the $r_{app}$ values were calculated from the measured reorganization energy values according to eq 8. The line represents a linear least-squares fit to data points 1−15. Miller's data represent the following redox probes (compounds 6, 8, and 15, ref 28; the remaining probes ref 40): (1) $[Fe(dMbpy)_3]^{3+}$; (2) $[Fe(bpy)_3]^{3+}$; (3) $[Ru(bpy)_3]^{3+}$; (4) $[Os(bpy)_3]^{3+}$; (5) $[Fe(dMbpy)_2(CN)_2]^{+}$; (6) $[Mo(CN)_8]^{3-}$; (7) *$[Fe(Sbpy)_2(CN)_2]^{-}$; (8) $[W(CN)_8]^{3-}$; (9) *$[Fe(Sbpy)_2(CN)_2]^{-}$; (10) $[Fe(bpy)_2(CN)_2]^{+}$; (11) $[Fe(CN)_6]^{3-}$; (12) $[Fe(Sbpy)(CN)_4]^{2-}$; (13) $[Fe(bpy)(CN)_4]^{-}$; (14) $[Fe(dMbpy)(CN)_4]^{-}$; (15) $[Ru(NH_3)_6]^{3+}$ (bpy = 2,2′-bipyridine; dMbpy = 4,4′-dimethyl-2,2′-bipyridine; Sbpy = 5-sulfonato-2,2′-bipyridine; (*) two stereoisomers of the complex).

to the alkyl chains at the monolayer/solution interface. Thus, the ferrocene moiety was not fully bathed by the aqueous environment.[26,53] In our case, the $\lambda$ value could be low due to a higher radius of our $FcCH_2N(CH_3)_3^{2+}$ relative to ferrocene itself. The larger $IrCl_6^{2-}$ reorganization energy in Table 1 is consistent with a smaller size of this probe. Thus, overall, both probes report aqueous environment. Therefore, their access to the electrode surface is restricted to a plane outside the Hg/$C_{16}$/solution interface.

While the comparison of the measured reorganization energies with the predictions of Marcus theory and the previous reports presents a clear picture of the position of the redox probes at the monolayer/solution interface, interpretation of the 6-fold difference in the $k_{app}(E)$ and $k_{app}^{max}$ values of the two probes (see Figure 5 and Table 1) is less straightforward. Since adsorption (driven by hydrophobic interactions) of the ferrocene probe at the interface could account for the observed difference,[54] we examined the concentration dependence of the apparent rate constants for $IrCl_6^{2-}$ and $FcCH_2N(CH_3)_3^{2+}$ over a $10^{-5}$ to $10^{-3}$ M range. This was done by chronoamperometry (as in Figure 3), and no dependence was found. Thus, neither probe appears to accumulate at the alkane/water interface. In the absence of such artifacts, the $k_{app}^{max}$ values should solely reflect the strength of the electronic coupling between a redox molecule and the electrode across a tunneling barrier. Since the barrier film and the underlying electrode material are in both cases the same, why is the ferrocene's $k_{app}^{max}$ value close to an order of magnitude higher than that obtained for $IrCl_6^{2-}$?

To answer this question, we examined the effect of the size of redox probes on the strength of electronic coupling. First, we note that, for the outer-sphere redox probes, $\lambda$ is a function of the probe's radius, $r$.[13,55]

$$\lambda \cong \frac{e^2}{32\pi\epsilon\epsilon_o r}\left(\frac{1}{\epsilon_{op}} - \frac{1}{\epsilon_s}\right) \qquad (8)$$

As mentioned above, the inverse relationship, $\lambda \propto 1/r$, and the data in Table 1 indicate that ferrocene probe is larger than $IrCl_6^{2-}$. Knowing that electron tunneling to $IrCl_6^{2-}$ and $FcCH_2N(CH_3)_3^{2+}$ involves metal-centered orbitals, electronic coupling in the later case should be slightly smaller (everything else being equal) since Fe of ferrocene is slightly further away from the electrode surface. This, of course, does not explain the opposite difference in the $k_{app}^{max}$'s in Table 1. Nevertheless, we sought to examine the validity of the $k_{app}^{max}$ vs $1/\lambda$ relationship. To do this, we correlated the literature values of the experimentally measured $k_{app}^{max}$'s for 15 different outer-sphere redox probes with their apparent radii, $r_{app}$ (radii were calculated from the measured $\lambda$ values). The data were published by Miller and coworkers who measured electron tunneling rates for these probes at gold electrodes coated with $\alpha,\omega$-hydroxytetradecanethiols.[28,40] They then determined the $k_{app}^{max}$ and $\lambda$ values using the same data analysis method we use in this report. A plot of Miller's data for the 15 probes in terms of $\ln(k_{app}^{max})$ vs $r_{app}$ is shown in Figure 6.[56] A good linear correlation strongly suggests that the electronic coupling between these probes and the electronic states in the metal electrode is sensitive to the differences in the proximity of the metal centers determined by the size of their ligand coordination sphere. The slope of this correlation yields a decay constant $\beta$ = 0.7 Å$^{-1}$. This value reflects the strength of electronic coupling through the various coordination spheres composed of five different ligands and their combinations, as shown in Figure 6. In view of the substantial structural and electronic differences in this collection of ligands, it is somewhat surprising that this correlation exists. To the extent that it does, it is analogous to the same general correlation described recently by Dutton for a large collection of redox proteins.[14] They both demonstrate the importance (if not dominance) of the distance in setting the magnitude of electronic coupling.

Unfortunately, our $k_{app}^{max}$ values for the ferrocene and iridium probes cannot be directly compared with Miller's data, since ours were obtained for monolayer films composed of longer alkanethiol molecules ($C_{16}$ vs $C_{14}$). However, we can attempt to correct our data for the two methylene group difference, knowing that the $k_{app}^{max}$ values are proportional only to the strength of electronic coupling and thus to the distance[13]

$$k_{app}^{max} = k_0^{max} \exp(-\beta d) \quad (9)$$

where $k_0^{max}$ is the maximum value of the heterogeneous electron-transfer rate constant expected for an uncoated electrode. Using $\beta = 1.1$ per $CH_2$ group obtained in our previous measurements,[24] we calculated the corrected values and plotted them vs $r_{app}$ (obtained from the measured $\lambda$'s) in Figure 6.[57] One can see that while ferrocene data fit reasonably well with Miller's series, the iridium's rate constant is low. In view of several approximations involved in this comparison, it is more important to focus on and to account for the relative difference between the two $k_{app}^{max}$ values obtained for our probes. To this end, we see two ways to account for this difference. One assumes that both probes arrive at the $Hg/C_{16}$/solution interface but that the ferrocene's concentration is higher due to adsorption. This possibility was all but eliminated by the independence of the $k_{app}$ values on the concentration of the redox probes. The other postulates that the difference is due to an inability of the $IrCl_6^{2-}$ ions to approach equally closely the $Hg/C_{16}$/solution interface. Specifically, a smaller value of $k_{app}^{max}$ for the iridium probe suggests that its approach to the alkane interface is restricted by a thin water layer. With $\beta_{water}$ of ca. 1.4 $Å^{-1}$, the 6-fold smaller $k_{app}^{max}$ for the $IrCl_6^{2-}$ corresponds to ca. 2 Å thick water layers.[6] This picture of more restricted access of the iridium probe to the alkane/water interface is consistent with a more hydrophilic character of this probe. Furthermore, inability of hydrophilic redox probes to penetrate the dynamically ordered water layer at the alkane/water interface was first observed in our earlier measurements of the electroreduction of $Ru(NH_3)_6^{3+}$ on Hg coated with alkanethiolate films and $\omega$-hydroxyalkanethiolate films.[24] In all cases of different hydrocarbon chain lengths, the rate of electron tunneling across nominally thicker hydroxy-terminated monolayers was actually *larger* than for the methyl-terminated films of the same number of carbon atoms. Overall, this explanation of the observed difference in the values of $k_{app}^{max}$ for the two probes suggests that adsorption of ferrocene at the $Hg/C_{16}$/solution interface indeed does not take place or that it is not very significant. Together with the difference of approach, an increase of the interfacial concentration of the ferrocene probe due to adsorption would result in a significantly larger difference in the $k_{app}^{max}$ values than those found experimentally and reported in Table 1.

**Location of the Redox Probes at the Alkane/Water Interface during Monolayer Expansion.** The use of a micrometrically driven HMDE allows us to investigate the blocking properties of monolayer films as a function of Hg drop expansion. In these experiments, a hexadecanethiolate monolayer is first formed on the Hg drop surface and the electrode is then thoroughly rinsed and transferred to an electrochemical cell filled with a hexadecanethiol-free aqueous electrolyte where kinetics of electron tunneling is investigated as a function of the applied potential for various degrees of Hg drop expansion.[24] To interpret correctly electron tunneling data obtained in such experiments, it is of critical importance to know the position of a redox probe at the monolayer/solution interface. In Figure 1, we presented two different scenarios each of which results in an increase of the measured tunneling rates with Hg drop expansion.[58] Clearly, a rate increase itself is not indicative of the mechanism that causes it. As shown below, determination of the reorganization energy of a probe at the monolayer/solution interface at each stage of monolayer expansion allows us to distinguish unambiguously between cases A and B in Figure 1.

The experimental approach and data analysis were outlined in the previous sections. Fast scan voltammetry was used to record current overpotential curves for the reduction of $IrCl_6^{2-}$ at a $Hg/C_{16}$ interface at progressively increasing stages of Hg drop expansion. Since current is proportional to the rate of electron transfer (equation 3), a set of $k_{app}$ vs $\eta$ can be readily obtained as shown in Figure 7A. The corresponding set of $dk_{app}/d\eta$ vs $\eta$ plots with the Gaussian fits are shown in Figure 7B. Quite clearly the position of the maxima and thus the $\lambda$ values are invariant with the monolayer expansion up to the maximum average tilt of the alkane chains of ca. 20°. This result proves that $IrCl_6^{2-}$ experiences the same aqueous environment throughout the entire sequence of the stepwise monolayer expansions. Clearly, $IrCl_6^{2-}$ follows case A in Figure 1. Expansion beyond ca. 25% of the original surface area results in monolayer fracture and an almost explosive current increase.

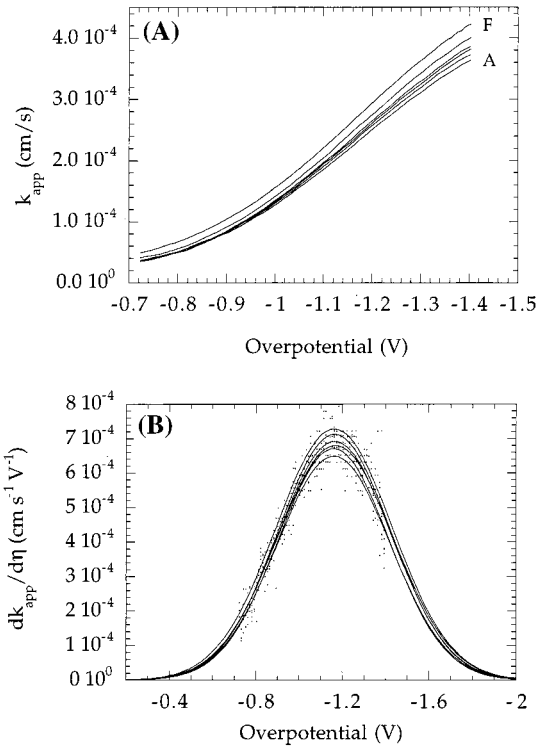


**Figure 7.** (A) The plots of $k_{app}$ vs overpotential for the reduction of $IrCl_6^{2-}$ at a hexadecanethiolate-coated Hg drop electrode as a function of its stepwise expansion. The curves A−F correspond to the electrode surface area of (A) 0.02458, (B) 0.02543, (C) 0.02628, (D) 0.02710, (E) 0.02792, (F) 0.02872 $cm^2$. The $i-V$ data were recorded under the condition of Figure 2. (B) The plots of $dk_{app}/d\eta$ vs $\eta$ and Gaussian fits corresponding to the data in part A.

Completely opposite behavior is observed in the case of a more hydrophobic ferrocene probe. Even a small expansion (∼2%) of the $Hg/C_{16}$ interface results in a very large increase of current and a destruction of the monolayer due to mercury oxidation. Thus, in this case, the monolayer is completely permeable by the $FcCH_2N(CH_3)_3^{2+}$ ions upon any attempt to expand it. Naturally, quantitative interpretation of this voltammetric behavior is impossible. These results support our postulates made in the previous section that the ferrocene probe can approach the alkane/solution interface more closely than $IrCl_6^{2-}$. Considering the differences in the behavior of the two probes, $FcCH_2N(CH_3)_3^{2+}$ is likely in a direct contact with the terminal methyl groups of the monolayer. This proximity to the alkane chains allows it to permeate the monolayer immediately upon its expansion. In contrast, a thin water layer that isolates $IrCl_6^{2-}$ from the alkane chains helps to maintain monolayer integrity and impermeability. More extensively hydrogen bonded

water at the alkane/water interface appears to play a structurally rigidifying role.[59]

## Conclusions

Presence of a hexadecanethiolate monolayer on a mercury drop electrode allows us to extend kinetic investigations of the electroreduction of kinetically facile redox probes such as $FcCH_2N(CH_3)_3^{2+}$ and $IrCl_6^{2-}$ into an otherwise inaccessible region of large overpotentials. When overpotential becomes comparable and then exceeds reorganization energy, kinetically controlled $i-\eta$ curves for these redox couples display curvature characteristic of the saturation region. Using the density of states approach we have determined the reorganization energies and the $k_{app}^{max}$ values for the two probes. We demonstrated that the $\lambda$ and $k_{app}^{max}$ values can be used as the diagnostic parameters revealing the location of a probe and the character of its solvent environment at the time of the electron transfer. Thus, full characterization of the kinetics of electron transfer between a redox probe and the monolayer-coated electrode surface provides not only information concerning the electronic coupling strength, a parameter characterizing the tunneling medium, but it also allows one to deduce the probe's local environment at the film/solution interface and to infer the structure of that interface. Specifically, comparison of the $k_{app}^{max}$ values suggests that the ferrocene probe is located more closely to the alkane/solution interface than $IrCl_6^{2-}$. This is consistent with a more hydrophilic nature of the iridium probe and its greater extent of hydration. This difference in the proximity of approach of the two probes of different hydrophobicity is strongly related to the character of the interface itself. Dynamically structured water at the alkane/water interface discriminates between hydrophilic and hydrophobic redox probes in the extent of their approach to the interface. This is not observed when hydroxylated alkanethiol monolayers are used. Our analysis of the kinetic data of Miller and co-workers obtained with the hydroxy-terminated monolayer films showed a good correlation of the $\ln(k_{app}^{max})$ vs $r_{app}$ for a number of hydrophilic and hydrophobic redox probes (Figure 6). This suggests that the proximity of all these probes to the hydrophilic interface is simply determined by their size. Also, we showed earlier that $Ru(NH_3)_6^{3+}$ can approach the hydroxylated alkanethiolate monolayers and that, as a result, these monolayers cannot be expanded without inducing permeation of the ruthenium probe through the monolayer.

Even more valuable are the experimental values of the reorganization energies of the ferrocene and iridium probes. Invariance of $\lambda(IrCl_6^{2-})$ with Hg drop expansion and thus with the increasing tilt of the alkane chains proves that $IrCl_6^{2-}$ does not enter the alkane region of the monolayer film (case A in Figure 1). According to our experiments, its position outside the monolayer is invariant with the monolayer expansion. Strikingly different results were obtained with the ferrocene probe. This more hydrophobic ions immediately permeate the monolayer when it is expanded even by ca. 2%.

**Acknowledgment.** Acknowledgment is made to the donors of the Petroleum Research Fund, administered by the ACS, for a partial support of this research. Additional support was provided by a grant from the National Science Foundation (CHE-942269). We also thank Dr. Cary J. Miller for discussing with us his experimental results.

## References and Notes

(1) Barbara, P. F.; Meyer, T. J.; Ratner, M. A. *J. Phys. Chem.* **1996**, *100*, 13248.
(2) Farver, O.; Pecht, I. *J. Biol. Inorg. Chem.* **1997**, *2*, 387.
(3) Beratan, D. N.; Skourtis, S. S. *Curr. Opinion Chem. Biol.* **1998**, *2*, 235.
(4) Boxer, S. G. *Annu. Rev. Biophys. Biophys. Chem.* **1990**, *19*, 267.
(5) Moser, C. C.; Page, C. C.; Farid, R.; Dutton, P. L. *J. Bioenerg. Biomembr*. **1995**, *27*, 263.
(6) Bendall, D. S., Ed. *Protein Electron Transfer*; BIOS Scientific Publishers Ltd.: Oxford, 1996.
(7) *Structure and Bonding: Long-Range Electron Transfer in Biology*; Springer-Verlag: New York, 1991; Vol. 75.
(8) Curry, W. B.; Grabe, M. D.; Kurnikov, I. V.; Skourtis, S. S.; Beratan, D. N.; Regan, J. J.; Aquino, A. J. A.; Beroza, P.; Onuchic, J. G. *J. Bioenerg. Biomembr*. **1995**, *27*, 285.
(9) Gray, H. B.; Winkler, J. R. *Annu. Rev. Biochem.* **1996**, *65*, 537.
(10) Grabert, H.; Devoret, M. H. In *Single Charge Tunneling, Coulomb Blockade Phenomena in Nanostructures*; Grabert, H., Devoret, M. H., Eds.; Plenum Press: New York, 1992.
(11) Aviram, A., Ratner, M., Eds. *Molecular Electronics: Science and Technology*; Ann. NY. Acad. Sci., 1998; Vol. 852.
(12) Jortner, J., Ratner, M., Eds. *Molecular Electronics;* IUPAC and Blackwell Science: Oxford, 1997.
(13) Marcus, R. A.; Sutin, N. *Biochim. Biophys. Acta* **1985**, *811*, 265.
(14) Moser, C. C.; Keske, J. M.; Warncke, K.; Farid, R. S.; Dutton, P. L. *Nature* **1992**, *355*, 796.
(15) Closs, G. L.; Miller, J. R. *Science* **1988**, *240*, 440.
(16) Kuki, A. Electronic Tunneling Paths in Proteins. *Structure and Bonding. Long-Range Electron Transfer in Biology*; Springer-Verlag: Berlin, 1991; p 49−84.
(17) Beratan, D. N.; Onuchic, J. N.; Winkler, J. R.; Gray, H. B. *Science* **1992**, *258*, 1740.
(18) Wuttke, D. S.; Bjerrum, M. J.; Winkler, J. R.; Gray, H. B. *Science* **1992**, *256*, 1007.
(19) Langen, R.; Chang, I.-J.; Germanas, J. P.; Richards, J. H.; Winkler, J. R.; Gray, H. B. *Science* **1995**, *268*, 1733.
(20) de Rege, P. J. F.; Williams, S. A.; Therien, M. J. *Science* **1995**, *269*, 1409.
(21) Finklea, H. O.; Liu, L.; Ravenscroft, M. S.; Punturi, S. *J. Phys. Chem.* **1996**, *100*, 18852.
(22) Cheng, J.; Saghi-Szabo, G.; Tossell, J. A.; Miller, C. J. *J. Am. Chem. Soc.* **1996**, *118*, 680.
(23) Slowinski, K.; Chamberlain, R. V.; Bilewicz, R.; Majda, M. *J. Am. Chem. Soc*. **1996**, *118*, 4709.
(24) Slowinski, K.; Chamberlain, R. V.; Miller, C. J.; Majda, M. *J. Am. Chem. Soc*. **1997**, *119*, 11910.
(25) Finklea, H. O. Electrochemistry of Organized Monolayers of Thiols and Related Molecules on Electrodes. *Electroanalytical Chemistry*; Bard, A. J., Rubinstein, I., Eds.; Marcel Dekker: New York, 1996; p 109−335.
(26) Chidsey, C. E. D. *Science* **1991**, *251*, 919.
(27) Smalley, J. F.; Feldberg, S. W.; Chidsey, C. E. D.; Linford, M. R.; Newton, M. D.; Liu, Y.-P. *J. Phys. Chem.* **1995**, *99*, 13141.
(28) Becka, A. M.; Miller, C. J. *J. Phys. Chem*. **1992**, *96*, 2657.
(29) Finklea, H. O.; Hanshew, D. D. *J. Am. Chem. Soc.* **1992**, *114*, 3173.
(30) Weber, K.; Hockett, L.; Creager, S. *J. Phys. Chem. B* **1997**, *101*, 8286.
(31) Dubois, L. H.; Nuzzo, R. G. Synthesis, Structure, and Properties of Model Organic Surfaces. *Annu. Rev. Phys. Chem*. **1992**, *43*, 437.
(32) Sachs, S. B.; Dudek, S. P.; Hsung, R. P.; Sita, L. R.; Smalley, J. F.; Newton, M. D.; Feldberg, S. W.; Chidsey, C. E. D. *J. Am. Chem. Soc*. **1997**, *119*, 10563.
(33) Creager, S.; Yu, C. J.; Bamdad, C.; O'Connor, S.; MacLean, T.; Lam, E.; Chong Y.; Olsen, G. T.; Luo, J.; Gozin, M.; Kayyem, J. F. *J. Am. Chem. Soc*. **1999**, *121*, 1059.
(34) Demoz, A.; Harrison, D. J. *Langmuir* **1993**, *9*, 1046.
(35) Bruckner-Lea, C.; Kimmel, R. J.; Janata, J.; Conroy, J. F. T.; Caldwell, K. *Electrochim. Acta* **1995**, *40*, 2897.
(36) Muskal, N.; Turyan, J.; Mandler, D. *J. Electroanal. Chem*. **1996**, *409*, 131.
(37) In these experiments, a micrometrically driven hanging mercury drop electrode was used. This device allows us to control the Hg drop size by increasing or decreasing the volume of the suspended drop with ca. 1% precision.
(38) Miller, C.; Cuendet, C. P.; Gratzel, M. *J. Phys. Chem*. **1991**, *95*, 877.
(39) Miller, C.; Gratzel, M. *J. Phys. Chem*. **1991**, *95*, 5225.
(40) Terrettaz, S.; Becka, A. M.; Traub, M. J.; Fettinger, J. C.; Miller, C. J. *J. Phys. Chem*. **1995**, *99*, 11216.
(41) Cheng, J.; Miller, C. J. *J. Phys. Chem. B* **1997**, *101*, 1058.
(42) Miller, C. J. Heterogeneous Electron-Transfer Kinetics at Metallic Electrodes. In *Physical Electrochemistry: Principles, Methods, and Applications*; Rubinstein, I., Ed.; M. Dekker: New York, 1995; p 27−79.
(43) Kemula, W.; Kublik, Z. *Anal. Chim. Acta* **1958**, *18*, 104.
(44) Becucci, L.; Moncelli, M. R.; Guidelli, R. *J. Electroanal. Chem.* **1996**, *413*, 187.

(45) Buoninsegni, F. T.; Herrero, R.; Moncelli, M. R. *J. Electroanal. Chem.* **1998**, *452*, 33.
(46) Magnussen, O. M.; Ocko, B. M.; Deutsch, M.; Regan, M. J.; Pershan, P. S.; Abernathy, D.; Gruebel, G.; Legrand, J.-F. *Nature* **1996**, *384*, 250.
(47) Saji, T.; Maryuyama, Y.; Aoyagui, S. *J. Electroanal. Chem.* **1978**, *86*, 219.
(48) Birkin, P. R.; Silva-Martinez, S. *Anal. Chem.* **1997**, *69*, 2055.
(49) Macpherson, J. V.; Jones, C. E.; Unwin, P. R. *J. Phys. Chem. B* **1998**, *102*, 9891.
(50) A comparison of the rates of mass transport and electron transfer can be made by calculating a magnitude of a diffusion-controlled voltammetric peak current that would be observed under the conditions of Figure 2 at a clean Hg drop electrode and then comparing that value to the maximum value of the observed current in Figure 2. The former is $i_p = (2.69 \times 10^5)A(D\nu)^{1/2}C^* = 1.67$ mA/cm$^2$ (obtained with $D(IrCl_6^{2-}) = 7.6 \times 10^{-6}$ cm$^2$/s). This value is 46 times higher than the highest current in (36.6 mA/cm$^2$) Figure 2.
(51) Bard, A. J.; Faulkner, L. R. *Electrochemical Methods, Fundamentals and Applications*; John Wiley & Sons*:* New York, 1980; Chapter 5.2, p 142.
(52) Fan, F.-R. F.; Bard, A. J. *Science* **1997**, *277*, 1791.
(53) Weber, K. S.; Creager, S. E. *J. Electroanal. Chem*. **1998**, *458*, 17.
(54) Becka, A. M.; Miller, C. J. *J. Phys. Chem*. **1993**, *97*, 6233.
(55) Equation 8 does not include the image charge effects since they are negligible for the purpose of the argument presented in the subsequent section in the text.
(56) The correlation in Figure 6 does not include Miller's data for $Ce^{4+}$ for which reorganization energy includes a substantial component of inner-sphere terms. Consequently, $\lambda(Ce^{4+})$ cannot be used to obtain a reliable value of the $Ce^{4+}$ radius.
(57) Since the monolayer films used by Miller and co-workers (ref 40) were hydroxy terminated, the difference between our hexadecanethiolate monolayer and their $\alpha,\omega$-hydroxytetradecanethiol monolayers is only one $\sigma$-bond. Thus, the correction we applied gives high estimates of the expected values. However, our previous measurements (ref 24) showed that the rates of electron tunneling across the hydroxy-terminated monolayer are actually somewhat higher than those measured at methyl terminated monolayers of the same number of carbon atoms. We also note that since Miller's data were obtained on gold electrode where the alkyl chains are tilted by ca. 30°, they are intrinsically higher than ours obtained on Hg (0° tilt angle), everything else being the same, due to a contribution to the total rate from a tunneling pathway involving chain-to-chain coupling. Thus, overall, the correction we used is reasonably accurate.
(58) We demonstrated previously that the increase of an electron tunneling rate in case A is due to additional contribution to the tunneling from a pathway involving chain-to-chain coupling (see ref 24).
(59) Sharp, K. A.; Madan, B. *J. Phys. Chem. B* **1997**, *101*, 4343.